A Conductive Nanowire-Mesh Biosensor for Ultrasensitive Detection of Serum C-Reactive Protein in Melanoma

*Zuan-Tao Lin, Yaxi Li, Jianhua Gu, Huie Wang, Zhuan Zhu, Xia Hong, Zijing Zhang, Qinqin Lu, Jingyi Qiu, Xifan Wang, Jiming Bao, and Tianfu Wu**

Detection of extracutaneous melanoma is still challenging and is of importance in improving survival rate. In this report, an ultrasensitive biosensor is constructed where a C-reactive protein (CRP) aptamers based molecular recognition core and a conductive polypyrrole (PPy) nanowire mesh based signal amplifier are developed. The conductive PPy nanowire (less than 10 nm in diameter) mesh architecture is uniformly dispersed within polymeric matrix via template-free in situ synthesis. Serum CRP levels are quantitatively analyzed through monitoring the conductance change caused by polymeric network shrinkage upon the aptamer-CRP binding. The limit of detection (LOD) of the polymeric sensor for human CRP sample can reach 7.85×10^{-19} M. This CRP-specific biosensor and a commercial CRP enzyme-linked immunosorbent assay (ELISA) kit are used to perform side-by-side measurement of serum CRP in melanoma patients. The results indicate that this conductive polymeric senor is highly sensitive and selective in accurately discriminating melanoma patients from healthy controls using serum CRP as a biomarker, which is further validated by a commercial human CRP ELISA kit. Collectively, this novel ultrasensitive nanowire-based polymeric biosensor may hold promise in biomarker detection and diagnosis of cancer.

1. Introduction

Melanoma, a malignant skin cancer, leads to an estimated 9730 death and ≈87 110 new cases in 2017.[1] The incidence of melanoma has been rising during the last 30 years, although the incidence of other cancers is decreasing.[2] Smartphone based imaging and Apps are emerging for detecting skin melanoma, but they are incapable of detecting extracutaneous melanomas which are located in the eyes, mouth, digestive tract, urinary tract, vagina or other internal organs.[3] The most effective approach to improve survival rate of melanoma is to establish an effective technology to enable accurate detection of circulating biomarkers of melanoma.

C-reactive protein (CRP) is considered as a biomarker generated by hepatocytes when inflammation occurs in body.[4] Recently, Fang et al. demonstrated that CRP could serve as an independent prognostic biomarker in melanoma patients.[5] The results showed that increased levels of CRP in plasma were correlated with disease stage in patients with melanoma.[5] In our previous studies, we reported a novel promising signal cascade strategy through an ultrasensitive polymeric sensor consisting of gold nanoparticles (gNPs)-decorated polymer in virtue of its superior sensitivity and electromechanical functionality.[6] The gNPs aggregation in polymeric network results in electrical conductance change upon specific aptamer-based biomolecular recognition.[6]

Intrinsically electrically conducting polymers (ICP) including polypyrrole (PPy)[7] and polyaniline (PANI)[8] are organic conducting polymers composed of polymeric monomers which become electrically conductive in polymeric network via oxidation or reduction.[9] In the past few decades, devices fabricated using ICP were widely investigated for biosensing applications.[10] More recently, a PPy-based conductive polymer with nanofiber structure and promising conductivity was synthesized using copper phthalocyanine-3,4′,4″,4‴-tetrasulfonic acid tetrasodium salt (CuPT) as a dopant counterion.[11] However, the applications based on ICP with high conductivity are severely limited by their poor mechanical properties and biocompatibility,[7a] which are major barriers for clinical applications.[9a,12] Conductive polymeric composites with the integration of biofunctionalized and stable polymers are attracting increasing attention and interest for their potentials in the development of biomedical devices.[10b,13]

In this report, as shown **Figure 1**a, first we synthesized a polymeric matrix by polymerizing acrylamide (AM),

Z.-T. Lin, Y. Li, Prof. X. Hong, Dr. Z. Zhang, Prof. Q. Lu, J. Qiu, Prof. T. Wu
Department of Biomedical Engineering
University of Houston
Houston, TX 77204, USA
E-mail: twu13@central.uh.edu

Dr. J. Gu, H. Wang
Electron Microscopy Core
Houston Methodist Research Institute
Houston, TX 77030, USA

Dr. Z. Zhu, Prof. J. Bao
Department of Electrical and Computer Engineering
University of Houston
Houston, TX 77204, USA

X. Wang
Department of Materials Science and NanoEngineering
Rice University
Houston, TX 77005, USA

The ORCID identification number(s) for the author(s) of this article can be found under https://doi.org/10.1002/adfm.201802482.

DOI: 10.1002/adfm.201802482

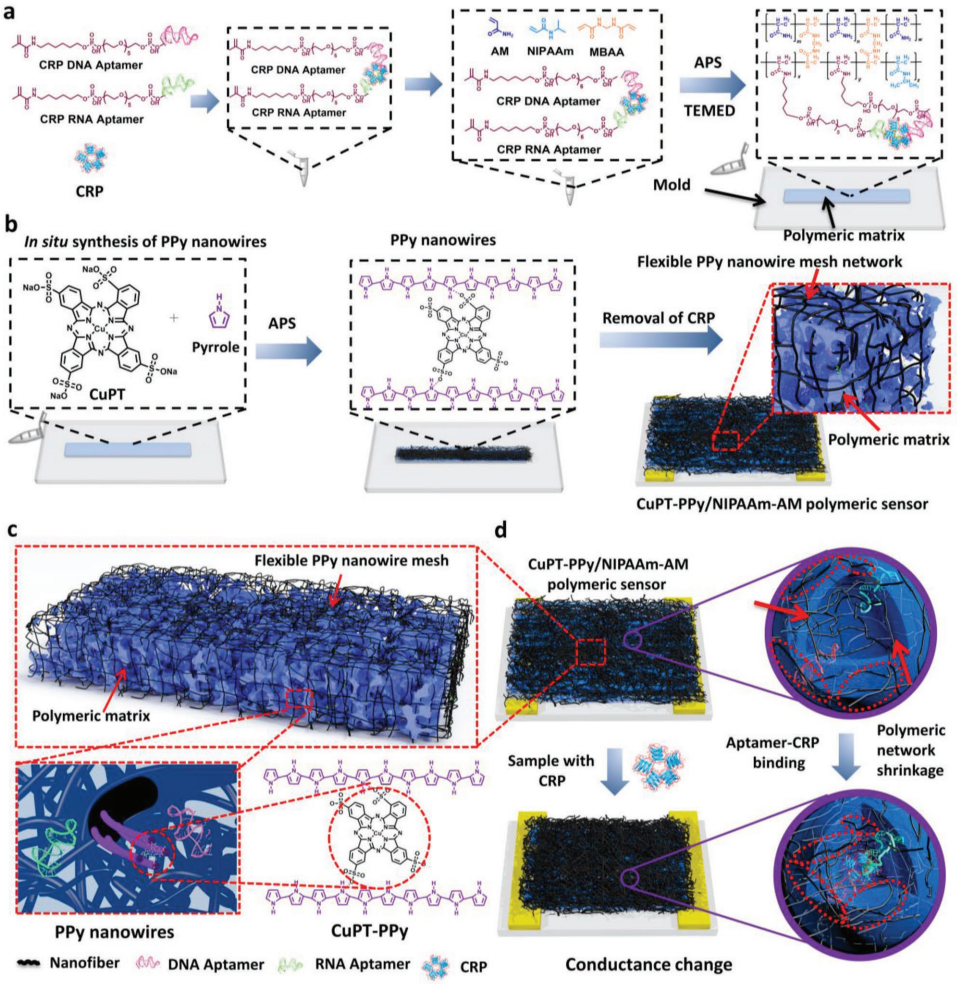

Figure 1. Design and fabrication of an ultrasensitive CuPT-PPy/NIPAAm-AM polymeric sensor. a) Synthesis of polymer with CRP recognition core (NIPAAm-AM-CRP-aptamer/CRP polymer). b) In situ synthesis of conductive polymeric nanowires (CuPT-PPy). c) Illustration of CuPT-PPy/NIPAAm-AM polymeric sensor and the conductive PPy nanowire mesh network structure of CuPT-PPy within the polymeric matrix. A molecular recognition core contains a pair of CRP DNA and RNA aptamers and the template CRP and CuPT-PPy nanowire mesh network are incorporated into the polymeric sensor. d) A molecularly imprinted cavity harboring a pair of aptamers specific for the CRP could be produced by removing the template CRP recombinant protein. During the assay, CRP-aptamer recognition and rebinding will induce polymeric network shrinkage, which cause deformation of the conductive nanowires mesh structure and cause electrical conductance change of the polymeric sensor.

methylenebisacrylamide (MBAA), *N*-Isopropylacrylamide (NIPAAm), and CRP/CRP-aptamers complex. Next, a flexible conductive mesh network architecture structure based on PPy was synthesized in situ using CuPT as a dopant counterion to form evenly dispersed nanowires within the NIPAAm-AM-CRP-aptamers/CRP polymeric matrix (Figure 1b,c). The template-free in situ synthesis of conductive polymer nanowire mesh is the first instance of fabrication of conductive polymer nanowire within polymer matrix. After removal of CRP recombinant protein from this complex, we were able to obtain a robust CuPT-PPy/NIPAAm-AM polymeric sensor for the detection of CRP with high sensitivity and selectivity. As shown in Figure 1b, this assay contains a two-step signal amplification cascade: 1) CRP binding-induced polymeric network shrinkage; 2) Conductance change of polymer caused by the shrinkage of the flexible conductive mesh network. This assay allows for quantitative analysis of serum CRP levels in patients by monitoring the changes in electrical conductance, which is promising for low-cost point-of-care applications.

2. Results and Discussion

The fabrication strategy of the CuPT-PPy/NIPAAm-AM polymeric sensor is shown in Figure 1. The NIPAAm-AM-CRP-aptamers/CRP polymer was synthesized first to provide a polymeric matrix of sensor with porous microstructure, followed by in situ polymerization and crosslinking of CuPT-PPy nanowires inside the porous polymeric matrix. It is essential to maintain the integrity of the biomolecule recognition core during the second step in the fabrication of polymeric sensor. Upon the removal of template molecules from the NIPAAm-AM-CRP-aptamers/CRP polymer, the nanowire might partially enter the cavities of the molecular imprint site and involve in

CRP-aptamers rebinding during the measurement. Thus, the template molecules should be removed after polymerization of CuPT-PPy nanowires in situ. Continuous transport path for electrons is of importance in the conductive polymer, especially for the stimuli responsive polymer. The porous microstructure NIPAAm-AM-CRP-aptamers/CRP polymer allows the aqueous solution of pyrrole monomer and dopant solution to immerse into the whole polymeric network. This would enable the PPy nanowires to disperse in the polymeric network uniformly. It is worth noting that the increased diameter of PPy nanowires can be achieved through the increase of reaction time.[11] Thus, we synthesized two types of polymeric sensors with different sizes of nanowires. Briefly, the regular CuPT-PPy/NIPAAm-AM polymer was designed and fabricated to have 10 nm nanowires in diameter after coating with 5 nm of Iridium, and the other one is named as CuPT-PPy/NIPAAm-AM polymeric sensor-100 which is composed of 100 nm nanowires in diameter. As a control, we also prepared a PA-PPy/NIPAAm-AM polymeric sensor using phytic acid (PA) as a crosslinker instead of CuPT.

Traditionally, PPy-based nanostructures and nanocomposites are synthesized either by oxidative polymerization or electrochemical polymerization of pyrrole with the aid of a template.[14] Preparation of a template, synthesis of PPy, and then removal of the template can be a complicated manufacturing process which is time-consuming and costly. Moreover, the template usually affects the properties of PPy. In contrast, our novel method of in situ synthesis of nanowires in polymeric matrix reported here is easy and fast. Furthermore, this method can be extended to the synthesis of other types of conductive nanowires. Therefore, this method may open up a new avenue for direct fabrication of conductive nanowire in substrate for broad applications, such as the fabrication of flexible electronics, soft robots, wearable devices, and electronic skins.

To examine the morphology and microstructure of the polymer samples, scanning electron microscopy (SEM) was employed and the results are shown in **Figure 2.** It is clear that the CuPT-PPy flexible network were formed in the NIPAAm-AM-CRP-aptamer/CRP polymeric matrix (Figure 2b,c,e,f). Since the samples were coated with 5 nm iridium, the average diameter of the nanowires of the network is about 10 nm. The nanowires spread as a network on the surface of the polymer, as well as inside the polymeric matrix network as shown in the cross-sectional images. When the in situ polymerization time was increased to 1 min, the average diameter of the nanowires was increased to 100 nm (Figure S1a, Supporting Information). Without CuPT as a dopant counterion, the PPy inside the polymeric sensor tended to form agglomerated and granular particles (Figure S1b, Supporting Information). Therefore, compared to the agglomerated structure of PA-PPy, the unique morphology structure of the PPy nanowire provides a larger surface area, which could benefit the transport of electrons. Hence, the signal amplification of conductance change of the polymeric sensor could be enhanced. Next, we employed atomic force microscopy (AFM) to further examine the nanostructure of PPy nanowires of the polymeric sensor. Interestingly, we could clearly appreciate the polymeric network formed by the PPy nanowires (**Figure 3**). Without metal coating, the average diameter of the nanowires is obviously smaller than that in the SEM images (Figure 2), but the overall PPy-nanowire structures are consistent in AFM and SEM.

As shown in Figure S2 (Supporting Information), the Fourier transform infrared (FTIR) spectra of NIPAAm-AM-CRP-aptamers polymer, CuPT-PPy, and CuPT-PPy/NIPAAm-AM polymeric sensor were used to analyze their functional groups. It is clear that a prominent amide II peak (N—H bending vibrations) at 1628 cm^{-1} and a strong amide I peak (C=O stretching vibrations) at 1665 cm^{-1} in the spectrum of NIPAAm-AM-CRP-aptamer

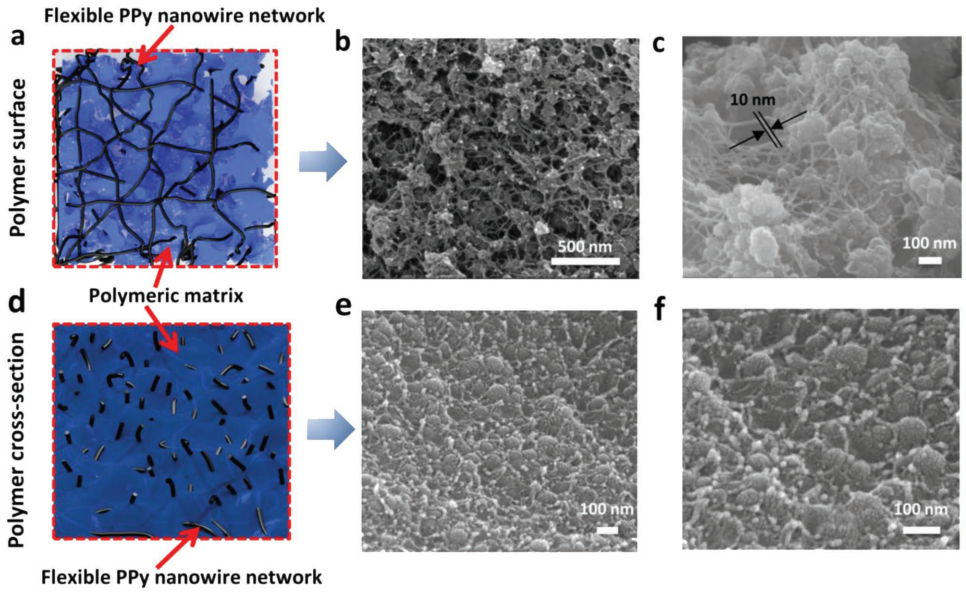

Figure 2. SEM images of the polymeric sensors. a) Schematic illustration of surface of the CuPT-PPy/NIPAAm-AM polymeric sensor. b,c) The surface of the CuPT-PPy/NIPAAm-AM polymeric sensor under different magnification (b, scale bar: 500 nm) (c, scale bar: 100 nm). d) Schematic illustration of cross-section of the CuPT-PPy/NIPAAm-AM polymeric sensor. e,f) Cross-section of the CuPT-PPy/NIPAAm-AM polymeric sensor under different magnification (e, scale bar: 100 nm) (f, scale bar: 100 nm).

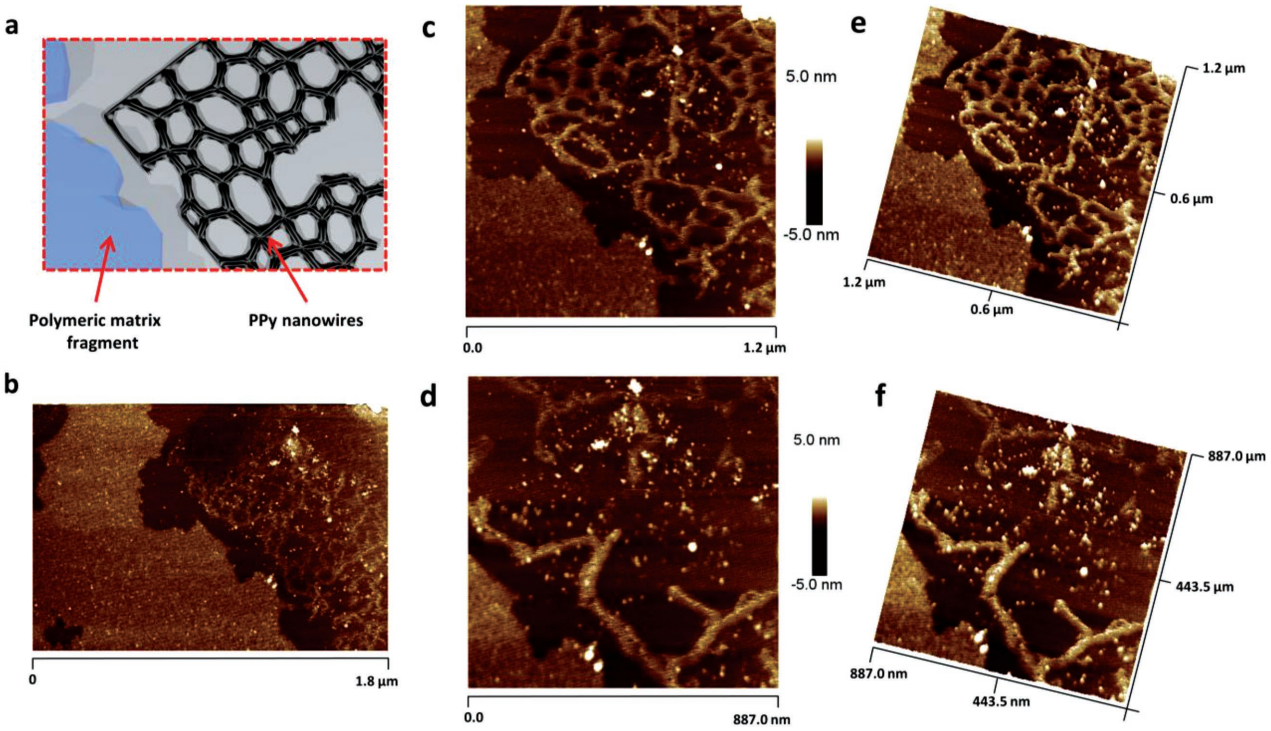

Figure 3. AFM analysis of the polymeric sensor. a) The schematic illustration of CuPT-PPy/NIPAAm-AM polymeric sensor structure after dehydration and sonication. b–d) The topography of CuPT-PPy/NIPAAm-AM polymeric sensor pieces at different magnifications and e,f) 3D AFM image corresponding to c,d) 2D AFM images. The polymeric matrix fragments and PPy nanowires are clearly observed. The "net-like" structure of the PPy-nanowire could not only provide conductivity but also facilitate volumetric changes of the sensor due to its superior flexibility.

polymer which are the characteristics of NIPAAm-AM, indicating the formation of NIPAAm-AM-aptamer copolymer.[15] In both spectra of CuPT-PPy and CuPT-PPy/NIPAAm-AM polymeric sensor, two absorption peaks at 1549 and 1475 cm^{-1} are assigned to the in-plane bending of C=N bonds and in-ring stretching of C=C bonds in the ring structure of PPy. Moreover, peaks at around 1039 cm^{-1} were due to the in-plane C—H and N—H bonds. It is noteworthy that two characteristic peaks corresponding to stretching vibrations of $C—N^+$ bonds and $C=N^+—C$ bonds at 1179 and 901 cm^{-1} can be found in both spectra of the material samples of CuPT-PPy and the CuPT-PPy/NIPAAm-AM polymeric sensor. This is in agreement with previous reports.[11] These results demonstrate that the CuPT-PPy nanowire was successfully synthesized in situ within the NIPAAm-AM-CRP-aptamers/CRP polymeric matrix.

We selected a pair of CRP-specific DNA and RNA aptamers which were validated by others,[16] and the sequences are presented in the "Materials" section in Experimental Section. To achieve the best performance of CuPT-PPy/NIPAAm-AM polymeric sensor, it is essential to optimize the CRP binding ability which is largely attributed to the concentration of the aptamers used for the construction of the molecular recognition of the sensor. CuPT-PPy/NIPAAm-AM polymeric sensor with various aptamer concentrations were prepared to examine the effect of aptamer concentrations. As shown in Figures S3–S5 in the Supporting Information, for both of CuPT-PPy/NIPAAm-AM polymeric sensor and CuPT-PPy/NIPAAm-AM polymeric sensor-100, when the aptamer concentrations were at 2.6×10^{-6} M, the polymeric sensor had the best performance. While for the PA-PPy/NIPAAm-AM polymeric sensor, when the aptamer concentrations were at 5.2×10^{-6} M, the polymeric sensor reached the maximum conductance change.

After slating the CuPT-PPy/NIPAAm-AM polymeric sensor, two natural landmarks "A" and "B" on the rough cross-section surface were selected by using in situ AFM measurement, and we were able to further investigate the dynamics of polymeric network shrinkage. Two natural landmarks "A" and "B" in **Figure 4** are corresponding to "A" and "B" on the cross-sectional height profile, as well as 2D and 3D topography image and (Figure 4a,c). As shown in Figure 4, the AFM topography and height profiles of the polymeric sensor were recorded and to analyze polymeric network shrinkage in response to phosphate-buffered saline (PBS) or CRP. There is almost no polymeric network shrinkage in the distance between the two landmarks "A" and "B" in both the cross-sectional height profile and topography images after incubation of PBS. However, it is apparent that a significant shrinkage of 9.56% was observed after the incubation with CRP samples. The distance between landmarks "A" and "B" decreases from 10.474 to 9.472 μm (Figure 4a–c).

To examine the sensitivity and specificity of the CuPT-PPy/NIPAAm-AM polymeric sensor, CuPT-PPy/NIPAAm-AM polymeric sensor-100, and PA-PPy/NIPAAm-AM polymeric sensor, various concentrations of human CRP, mouse CRP, human thrombin, and bovine serum albumin (BSA) solutions in a range from 10^{-20} to 10^{-6} M in PBS were used to establish the binding kinetics as shown in **Figure 5**a–c. For both CuPT-PPy/NIPAAm-AM polymeric sensor and CuPT-PPy/NIPAAm-AM

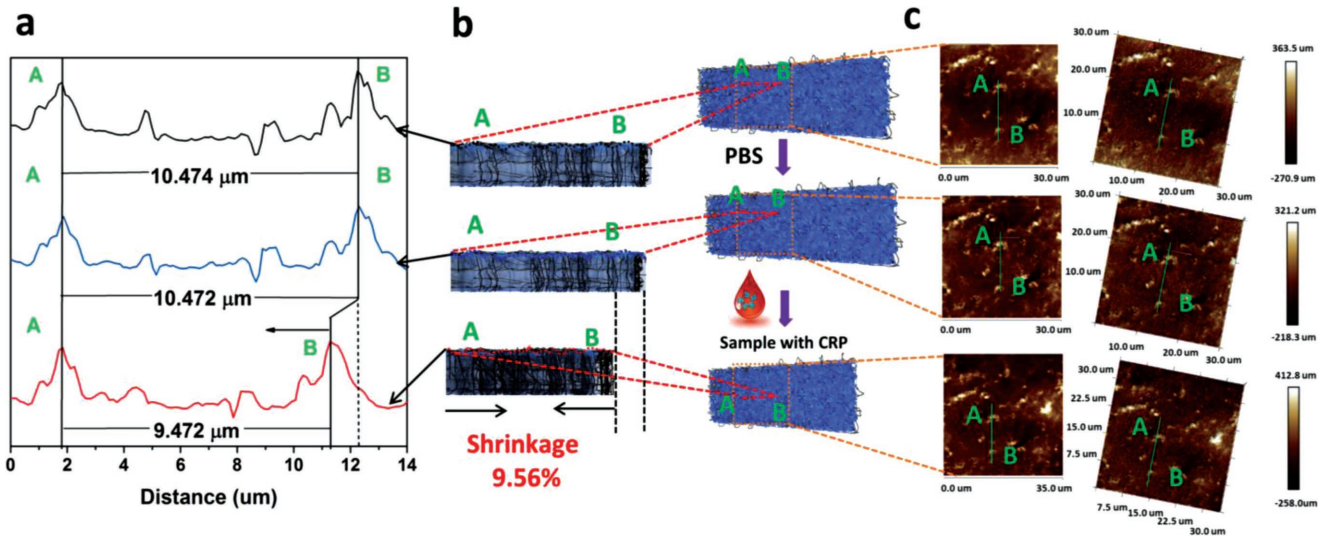

Figure 4. In situ AFM imaging of PPy-nanowire-based polymeric sensor. To measure the polymeric network shrinkage responses of the sensor (CuPT-PPy/NIPAAm-AM polymeric sensor) after the addition of CRP or PBS, we slated the polymer sensor and selected two natural landmarks (A and B) on the rough surface of cross-section of the polymer. a) The high profile derived from AFM topography was used to analyze the distance change between landmark A and B. b) Illustration of in situ AFM topography study. c) 2D and 3D in situ AFM topography images of the polymeric sensor before and after adding PBS or 1×10^{-8} M CRP.

polymeric sensor-100, the limit of detection (LOD) for human CRP could reach 7.85×10^{-19} M (9.03×10^{-17} g mL^{-1}) and 8.32×10^{-19} M (9.56×10^{-17} g mL^{-1}) in PBS. However, the LOD of PA-PPy/NIPAAm-AM polymeric sensor is 9.61×10^{-18} M (1.11×10^{-15} g mL^{-1}) in PBS. This polymeric sensor exhibited superior sensitivity to the commercial enzyme-linked immunosorbent assay (ELISA) kit (LOD: 15.60 pg mL^{-1}). Moreover, Table S1 (Supporting Information) summarized the functionality comparison of existing CRP assays and our sensor result. To date, it is obvious that our sensor has the lowest LOD. Upon the addition of CRP solution at 10^{-8} M, the highest electrical conductance change using CuPT-PPy/NIPAAm-AM polymeric sensor, CuPT-PPy/NIPAAm-AM polymeric sensor-100, and PA-PPy/NIPAAm-AM polymeric sensor were 365.03 ± 13.91%, 179.62 ± 12.37%, and 132.62 ± 7.01%, respectively. It is notable that the highest electrical conductance change of CuPT-PPy/NIPAAm-AM polymeric sensor is 2.75-fold higher than that of PA-PPy/NIPAAm-AM polymeric sensor, while highest electrical conductance change of CuPT-PPy/NIPAAm-AM polymeric sensor is 2.03-fold higher than that of CuPT-PPy/NIPAAm-AM polymeric sensor-100. This may be because the dopant CuPcTs enhanced the interchain charge transport of PPy, leading to dramatically improved conductivity compared with the PPy which was crosslinked by PA. Besides, compared to the gold nanoparticle-decorated sensor we reported previously,[6] the conductance change is increased. Furthermore, mouse CRP (sharing 71% homology to human CRP), human thrombin, BSA were used as negative control to examine the selectivity of sensor. The electrical conductance change for both sensors was at baseline levels in the presence of the negative control proteins, indicating that both polymeric sensors exhibited great specificity.

To evaluate the clinical potential of the conductive CuPT-PPy/NIPAAm-AM polymeric sensor developed in this study, a pilot study measuring CRP levels in serum samples from patients with melanoma was carried out. Briefly, serum samples from melanoma patients (N = 20) and healthy donors (N = 10) were properly diluted for the sensor assay so that all measurements fall into the range of the standard curve as established in **Figure 6**a. To validate the results determined from the CuPT-PPy/NIPAAm-AM polymeric sensor, a commercial ELISA kit for detection of Human CRP was utilized to test the same blood samples. Similar results were achieved from the test using a commercial ELISA kit as shown in Figure 6b. Next, we performed a paired correlation analysis of the results between ELISA and CuPT-PPy/NIPAAm-AM polymeric sensor, i.e., the data obtained from the same patient using sensor assay or ELISA were used for pair test of correlation. As shown in in Figure 6c, a strong correlation with a R^2 value of 0.9765 was found between sensor and ELISA. These results demonstrate that the CuPT-PPy/NIPAAm-AM polymeric sensor can provide reliable and accurate results in measuring serum CRP in melanoma patients. We also performed the same experiment using CuPT-PPy/NIPAAm-AM polymeric sensor-100, and the results are shown in Figure S6 (Supporting information). Likewise, the correlation between CuPT-PPy/NIPAAm-AM polymeric sensor-100 and ELISA was also strong, with a R^2 value of 0.9370 (Figure S6 in the Supporting Information).

In virtue of the polymeric network structure and the use of aptamers, the process of CRP binding-removal-rebinding enables the reproducibility of the polymeric sensor. We then tested the reproducibility the CuPT-PPy/NIPAAm-AM polymeric sensor. The results showed in Figure S7 (Supporting Information) indicate that the CuPT-PPy/NIPAAm-AM polymeric sensor assay is reproducible and reliable even after six additional CRP binding-removal-rebinding cycles in the presence of 1×10^{-8} M of CRP (in PBS buffer).

The results of the CRP detection reveal that the nanostructure of PPy plays an essential role in the conductance change responses upon CRP binding. The performance of polymeric sensors composed of PPy with nanowires structure is better

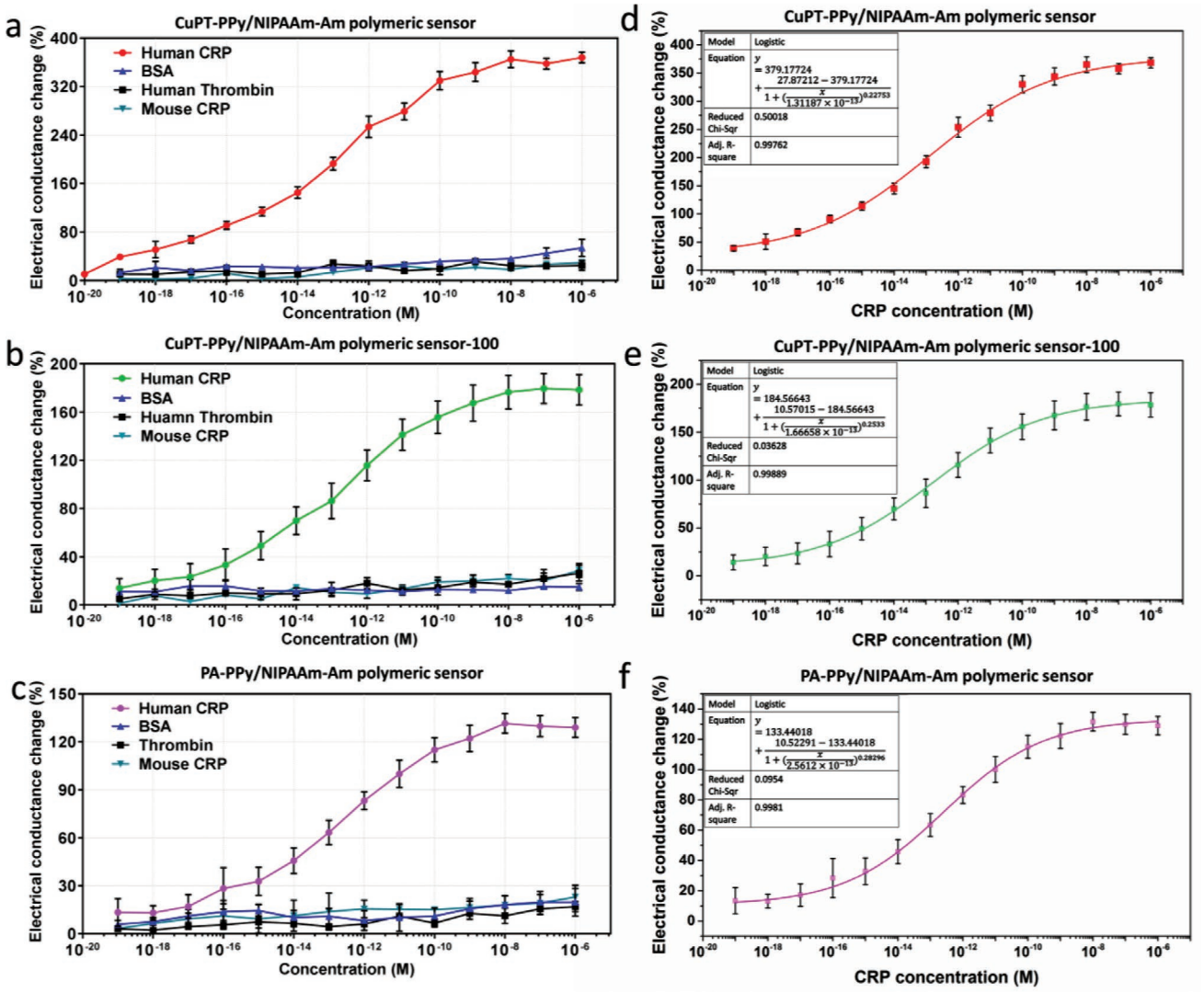

Figure 5. a–c) Kinetics of polymeric sensor responses to various concentrations of human CPR in PBS in three different sensors. Mouse CRP (71% homology), human thrombin, and BSA were used as negative controls. d–f) Nonlinear logistic fitting was performed for each sensor.

than that with granular nanoparticles (Figure S8, Supporting Information). The steric effect generated by the tetrasulfonic acid functional groups of CuPT promotes one dimensional PPy chain to be connected and grown into ordered nanowire structure. Besides the interchain charge transport of PPy mentioned above, the semiconductor property of copper phthalocyanine

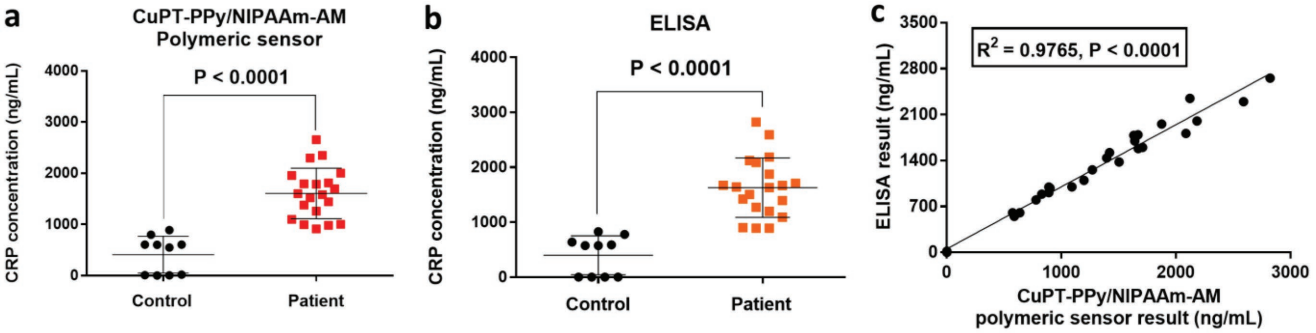

Figure 6. a) The CuPT-PPy/NIPAAm-AM polymeric sensor was used to measure a melanoma biomarker CRP in a serum from melanoma patients ($N = 20$) and healthy controls ($N = 10$). b) The same serum samples were used to measure serum CRP levels with a commercial human CRP ELISA kit. c) The paired correlation test was performed for the CuPT-PPy/NIPAAm-AM polymeric sensor results versus the ELISA results.

molecule also enhances the conductivity of the primary PPy chain, while the PA is an insulator.[11] However, compared to PA-PPy/NIPAAm-AM polymeric sensor, the performance of CuPT-PPy/NIPAAm-AM polymeric sensor-100 did not increase dramatically. This might be due to the aggregation of granular nanoparticles caused by the polymeric network shrinkage upon the response to the CRP-aptamer binding, which is similar to the polymeric sensor containing gold nanoparticles as described in our previous studies.[6] When the size of the PPy nanowire was reduced, the conductance change had a significant increase. Importantly, it is obvious that the PPy conductive flexible network plays a key role in this two-step signal amplification cascade. Therefore, the nanosized PPy fibers could constitute a conductive network in the polymeric matrix which is flexible and robust in volumetric changes when responding to the binding of target molecules.

On the other hand, the performance of sensors is strongly affected by the binding site produced by CRP-aptamer recognition core. Interestingly, the optimal aptamer concentration of PA-PPy/NIPAAm-AM polymeric sensor is twofold higher than that of CuPT-PPy/NIPAAm-AM polymeric sensor. Although the aggregation of granular nanoparticles of PPy could cause the conductance changes of the polymeric sensor, it requires more binding sites to obtain the optimal performance. In addition, since ELISA assay is time-consuming, tedious, and highly dependent on large equipment such as plate washer and plate reader, this polymeric sensor can obviously provide an alternative approach for point-of-care in rapid detection of melanoma. This study has demonstrated the proof of concept of a flexible PPy-nanowire network based polymeric sensor in biomarker detection. The flexibility of the sensor allows for rational redesign and synthesis to adapt to the detection of various biomarkers including CRP in the body fluids (e.g., blood, urine) in the diagnosis of various other diseases in addition to melanoma.

3. Conclusions

In summary, we developed an ultrasensitive polymeric sensor based on PPy flexible conductive network-decorated polymeric composites to detect a melanoma cancer biomarker–CRP in blood samples of melanoma patients. The FTIR spectra show that the conductive nanowire mesh was in situ synthesized in the polymeric sensor matrix successfully. SEM and AFM images reveal that PPy nanowires were dispersed uniformly and formed a mesh architecture on the surface and within the polymeric matrix. The kinetics of CRP binding to a CuPT-PPy/NIPAAm-AM polymeric sensor was investigated. This conductive polymeric biosensor exhibited a great sensitivity, selectivity, and accuracy in measuring serum levels of CRP in patients with melanoma. It is important to point out that high sensitivity is the key for early diagnosis. Indeed the advantage of this sensor lies in its superior sensitivity compared to ELISA or other sensors as summarized in Table S1 (Supporting Information). In this study we used CRP to demonstrate the proof of concept of our novel sensor; however, for eventual early diagnosis, we will need to measure a melanoma-specific "early biomarker" once it is clinically available.

4. Experimental Section

Materials: Recombinant human CRP was purchased from Lee BioSolution (Maryland Heights, MO, USA). A pair of linker modified human CRP-specific RNA and DNA aptamers: (TTTTTGCCUGUAAGGUGGUCGGUGUGGCGAGUGUGUUAGGAGAGAUUGC and TTTTTGGCAGGAAGACAAACACGATGGGGGGGTATGATTTGATGTGGTTGTTGCATGATCGTGGTCTGTGGTGCT)[16] were synthesized by Integrated DNA Technologies (Coralville, IA, USA). Human C-Reactive Protein (CRP) DuoSet ELISA Kit was obtained from R&D System (Minneapolis, MN, USA). CRP recombinant mouse protein was obtained from Thermo Fisher Scientific (Waltham, MA, USA). Human α-thrombin was purchased from Haematologic Technologies (Essex Junction, VT, USA). Pyrrole, CuPT, PA, AM, MBAA, NIPAAm, *N,N,N′,N′*-tetramethylethylenediamine (TEMED), guanidinium hydrochloride, BSA, sodium acetate, were purchased from Sigma-Aldrich (St. Louis, MO, USA). PBS was obtained from Life Technologies (Carlsbad, CA, USA). Sodium dodecylsulfate (SDS) was purchased from Strem Chemicals (Newburyport, MA, USA). Ammonium persulfate (APS) was obtained from Amresco (Solon, OH, USA). Ethyl alcohol was obtained from Pharmco-AAPER (Shelbyville, KY). All distilled water used in this study was generated using a Thermo Scientific Barnstead GenPure water purification system (Waltham, MA, USA).

Clinical samples: Serum samples from Melanoma patients ($N = 20$) as well as normal controls ($N = 10$) were provided by Dr. Shenying Fang and Dr. Stephen Tyring (Center for Clinical Studies, Houston, Texas). The sample collection was performed under an institutional approved IRB protocol. All samples were aliquoted and stored at –80 °C until use.

Synthesis of Polymer with a CRP Recognition Core (NIPAAm-AM-CRP-aptamers/ CRP Polymer): First, the acrylated CRP-specific DNA and RNA aptamers were dissolved in the PBS and stored at –20 °C. 13.06 µL of CRP (5 mg mL^{-1}) and 10 µL of DNA aptamer and RNA aptamer (2.6×10^{-5} M) were mixed for 30 min to fabricate the CRP biomolecular recognition core. Next, AM (12 mg) and NIPAAm (7.4 mg) were added to the above solution followed by the addition of 8 µL of MBAA (2%). Then, PBS and APS (10%, 44 µL) was added to make the mixture volume to 100 µL. Argon was used to degas the solution for 5 min. Next, 0.6 µL of TEMED was added and mixed with the resultant mixture, and then it was immediately transferred into a sensor mold (2.5 mm × 25 mm × 0.2 mm) for polymerization. The polymer in the mold was then immersed in PBS for rehydration and was peeled off. For removal of the unreacted reagents, PBS solution was used to wash the sensor and changed every 15 min (five times). The resultant polymer was then cut into desired sizes.

In Situ Synthesis of Conductive Polymeric Sensors: The polymeric sensors based on PPy-decorated polymer composites with CRP recognition core was prepared according to the method with modification in previous study.[11,17] Briefly, the obtained NIPAAm-AM-CRP-aptamers/CRP polymer was dehydrated under vacuum and immersed in pyrrole solution (40 mg mL^{-1}). For fabrication of polymeric sensors using phytic acid as crosslinker (PA-PPy/NIPAAm-AM polymeric sensor), the rehydrated polymer with CRP recognition core was then added into 1 mL of PA solution containing 28 mg of APS. For fabrication of polymeric sensors using CuPT as crosslinker (CuPT-PPy/NIPAAm-AM polymeric sensor), the rehydrated polymer with CRP recognition core was then added into solution containing 0.015 g of CuPT and 0.14 g of APS in 1 mL of distilled water. The resultant polymeric sensors were immersed in PBS solution to remove the unreacted reagents.

Removal of Template Biomolecules from the Polymeric Sensor: A washing buffer containing 4.3 M guanidinium hydrochloride, 1.4 M NaCl, and 0.1% SDS was prepared. The template molecules were removed from the polymeric sensor using washing solution with agitation on vortex every 15 min for a total of five times.

Quantify Removal Rate of CRP from the Polymeric Sensor: The washing solution was collected during the process of removal of CRP form the polymeric sensor and was used to calculate the removal rate of CRP via. Next, we measured CRP fractions in the washing buffer using a human CRP ELISA kit as detailed in the "Validation Assay" section to quantify removal rate of CRP from the polymeric sensor.

Fourier Transform Infrared (FT-IR) Spectroscopy Analysis: The samples after dehydration were mixed with potassium bromide and were pressed into a plate. The spectra of the material samples were performed on a Nicolet 6700 infrared spectrometer (Thermo Fisher Scientific, Waltham, MA, USA).

Scanning Electron Microscopy (SEM) Analysis: The polymeric sensors were sequentially immersed in ethanol and dried under vacuum. The dried samples were then broken into pieces, and coated with 5 nm of iridium. A Nova NanoSEM 230 (FEI, Hillsboro, OR, USA) was employed to carry out the cross-sectional SEM images of the polymeric sensor.

Atomic Force Microscopy (AFM) Measurement: The polymeric sensors were sequentially immersed in ethanol and dried dehydrated by a Tousimis supercritical point dryer (Rockville, MD, USA) using liquid carbon dioxide as the transitional fluid, following by sonication in degassed alcohol using Qsonica Q125 sonicator (Newtown, CT, USA). A MultiMode AFM (Bruker, Billerica, MA, USA) was used to determine the nanostructure of PPy nanowires of the polymeric sensor. The topography of polymeric sensor was carried out by using an AFM probe with a soft silicon nitride cantilever and tips (Bruker, spring constant of 0.01 N m^{-1}; Model: MLCT). NanoScope analysis version 1.50 software (Bruker, Billerica, MA, USA) was used for the analysis AFM images.

In Situ AFM Imaging of PPy-Nanowire Based Polymeric Sensor: Briefly, the polymeric sensor was immobilized on a polydimethylsiloxane (PDMS) film, allowing the AFM tip to scan the rough surface of the sensor. As shown in Figure 4, the topography of an area containing two representative natural landmarks ("A" and "B") on its rough surface was selected and recorded before and after addition of PBS or sample with CRP. In situ AFM measurements were performed on a MultiMode AFM (Bruker, Billerica, MA, USA) in a PeakForce QNM (quantitative nanoscale mechanical) mode by utilizing an AFM probe with a soft silicon nitride cantilever and silicon nitride tips (Bruker, spring constant of 0.01 N m^{-1}; Model: MLCT). The topography scanning was carried out under ≈95% relative humidity at room temperature. After the addition of samples containing CRP, the polymeric network shrinks, followed by the decrease of distance of longitudinal topography of two representative natural landmarks. Topography analysis of AFM images and height profiles was performed using NanoScope Analysis Version 1.50 software (Bruker, Billerica, MA, USA).

Sensor Assay: To examine the sensitivity and selectivity of the synthesized polymeric sensors, various concentrations of CRP or BSA solution ranging between 10^{-20} and 10^{-6} M were prepared in PBS. After removal of the template CRP, the as-synthesized polymeric sensors were incubated with each sample for 15 min. And then, the sensor was placed into PBS for 4 min to remove the unbound CRP. The electrical resistance of the polymeric sensor was detected under 95% relative humidity at room temperature using a Keithley 2450 source meter (Keithley Instruments, Cleveland, OH, USA).

Validation Assay: Serum CRP levels of the melanoma patients were measured using a human CRP ELISA DuoSet kit (R&D Systems, Minneapolis, MN, USA). The assay was performed following the manufacturer's instructions. The ELISA plates were read using a UV spectrophotometer (Epoch, Biotek, Winooski, VT, USA). The data was analyzed using Graphpad Prism 7.

Reproducibility and Reusability of Polymeric Sensor: To test the robustness of the sensor after the removal of CRP, reproducibility and reusability test of the sensor was performed. Briefly, the polymeric sensor with 1×10^{-8} M CRP was incubated and the conductance changes were measured, then removed the CRP using the method described above, and then the sensor was washed with PBS to remove the residual salts. Next, the sensor will be incubated in 1×10^{-8} M CRP for rebinding and assay. This binding–removal–rebinding cycle was repeated for ten times.

Long-Term Stability Study: To investigate the long-term stability of PPy nanowire sensor, the CuPT-PPy/NIPAAm-AM polymeric sensor was tested upon the addition of 1×10^{-8} M CRP in PBS. Next, the target CPR bounded in polymeric sensor was removed from the polymeric sensor using washing solution with agitation on a vortexer every 15 min for a total of five times, followed by drying under vacuum and then stored in a sealing box in black at room temperature. After six months, this PPy nanowire sensor was tested upon the addition of 1×10^{-8} M CRP in PBS again.

Supporting Information

Supporting Information is available from the Wiley Online Library or from the author.

Acknowledgements

This study was partly supported by a startup fund from the University of Houston (to T.W.) and a research grant from the Lupus Research Alliance (to T.W.). The authors acknowledge Dr. Shenying Fang and Dr. Stephen Tyring (Center for Clinical Studies, Houston, Texas) for providing clinical samples. Additional support was from Robert A. Welch Foundation (E-1728, to J.B.).

Conflict of Interest

The authors declare no conflict of interest.

Keywords

biomarkers, biosensors, melanoma, nanowire mesh, polypyrrole

Received: April 11, 2018
Published online:

[1] A. G. Sauer, R. L. Siegel, A. Jemal, S. A. Fedewa, *Cancer Epidemiol. Biomarkers Prev.* **2017**, *26*, 1192.
[2] R. L. Siegel, K. D. Miller, S. A. Fedewa, D. J. Ahnen, R. G. Meester, A. Barzi, A. Jemal, *CA-A Cancer J. Clin.* **2017**, *67*, 177.
[3] a) N. A. Ferrero, D. S. Morrell, C. N. Burkhart, *J. Am. Acad. Dermatol.* **2013**, *68*, 515; b) J. A. Wolf, J. F. Moreau, O. Akilov, T. Patton, J. C. English, J. Ho, L. K. Ferris, *JAMA Dermatol.* **2013**, *149*, 422.
[4] K. H. Allin, B. G. Nordestgaard, *Crit. Rev. Clin. Lab. Sci.* **2011**, *48*, 155.
[5] S. Fang, Y. Wang, D. Sui, H. Liu, M. I. Ross, J. E. Gershenwald, J. N. Cormier, R. E. Royal, A. Lucci, C. W. Schacherer, *J. Clin. Oncol.* **2015**, *33*, 1389.
[6] Z. T. Lin, J. Gu, C. H. Li, T. R. Lee, L. Xie, S. Chen, P. Y. Cao, S. Jiang, Y. Yuan, X. Hong, H. Wang, D. Wang, X. Wang, G. B. Jiang, M. Heon, T. Wu, *Adv. Mater.* **2017**, *29*, 1702090.
[7] a) R. Jain, N. Jadon, A. Pawaiya, *TrAC, Trends Anal. Chem.* **2017**, *97*, 363; b) S. Pruneanu, S. A. F. Al-Said, L. Dong, T. A. Hollis, M. A. Galindo, N. G. Wright, A. Houlton, B. R. Horrocks, *Adv. Funct. Mater.* **2008**, *18*, 2444; c) H. Okuzaki, T. Kuwabara, K. Funasaka, T. Saido, *Adv. Funct. Mater.* **2013**, *23*, 4400; d) X. He, C. Li, F. Chen, G. Shi, *Adv. Funct. Mater.* **2007**, *17*, 2911; e) L. Pan, A. Chortos, G. Yu, Y. Wang, S. Isaacson, R. Allen, Y. Shi, R. Dauskardt, Z. Bao, *Nat. Commun.* **2014**, *5*, 3002; f) A. Al-Mokaram, M. A. Amir, R. Yahya, M. M. Abdi, H. N. M. E. Mahmud, *Nanomaterials* **2017**, *7*, 129.
[8] D. Zhai, B. Liu, Y. Shi, L. Pan, Y. Wang, W. Li, R. Zhang, G. Yu, *ACS Nano* **2013**, *7*, 3540.
[9] a) Y. Zhao, L. Cao, L. Li, W. Cheng, L. Xu, X. Ping, L. Pan, Y. Shi, *Sensors* **2016**, *16*, 1787; b) A. Ramanavičius, A. Ramanavičienė, A. Malinauskas, *Electrochim. Acta* **2006**, *51*, 6025; c) J. Zhang,

L. Zhong, Y. Sun, A. Li, J. Huang, F. Meng, B. K. Chandran, S. Li, L. Jiang, X. Chen, *Adv. Mater.* **2016**, *28*, 2978; d) P. M. Nia, W. P. Meng, F. Lorestani, M. Mahmoudian, Y. Alias, *Sens. Actuators, B* **2015**, *209*, 100; e) Y. Yang, A. M. Asiri, D. Du, Y. Lin, *Analyst* **2014**, *139*, 3055; f) T. Kangkamano, A. Numnuam, W. Limbut, P. Kanatharana, T. Vilaivan, P. Thavarungkul, *Biosens. Bioelectron.* **2018**, *102*, 217.

[10] a) M. Xue, F. Li, D. Chen, Z. Yang, X. Wang, J. Ji, *Adv. Mater.* **2016**, *28*, 8265; b) J. W. To, J. He, J. Mei, R. Haghpanah, Z. Chen, T. Kurosawa, S. Chen, W.-G. Bae, L. Pan, J. B.-H. Tok, *J. Am. Chem. Soc.* **2016**, *138*, 1001; c) M. Li, H. Li, W. Zhong, Q. Zhao, D. Wang, *ACS Appl. Mater. Interfaces* **2014**, *6*, 1313; d) H.-K. Jun, Y.-S. Hoh, B.-S. Lee, S.-T. Lee, J.-O. Lim, D.-D. Lee, J.-S. Huh, *Sens. Actuators, B* **2003**, *96*, 576; e) V. Venugopal, V. B. Sundaresan, *J. Intell. Mater. Syst. Struct.* **2016**, *27*, 1702; f) H. Niu, H. Zhou, H. Wang, T. Lin, *Macromol. Mater. Eng.* **2016**, *301*, 707; g) S. Bagchi, C. Ghanshyam, *J. Phys. D: Appl. Phys.* **2017**, *50*, 105302; h) K. Dunst, K. Cysewska, P. Kalinowski, P. Jasiński, *IOP Conf. Ser.: Mater. Sci. Eng.* **2016**, *104*, 012028; i) J. S. Lee, D. H. Shin, J. Jun, J. Jang, *ACS Nano* **2013**, *7*, 10139; j) O. S. Kwon, S. J. Park, J.-Y. Hong, A.-R. Han, J. S. Lee, J. S. Lee, J. H. Oh, J. Jang, *ACS Nano* **2012**, *6*, 1486; k) N. German, A. Kausaite-Minkstimiene, A. Ramanavicius, T. Semashko, R. Mikhailova, A. Ramanaviciene, *Electrochim. Acta* **2015**, *169*, 326.

[11] Y. Wang, Y. Shi, L. Pan, Y. Ding, Y. Zhao, Y. Li, Y. Shi, G. Yu, *Nano Lett.* **2015**, *15*, 7736.

[12] a) R. Ravichandran, S. Sundarrajan, J. R. Venugopal, S. Mukherjee, S. Ramakrishna, *J. R. Soc., Interface* **2010**, *7*, S559; b) E. A. Della Pia, J. V. Holm, N. Lloret, C. Le Bon, J.-L. Popot, M. Zoonens, J. Nygård, K. L. Martinez, *ACS Nano* **2014**, *8*, 1844; c) S. Brahim, D. Narinesingh, A. Guiseppi-Elie, *Biosens. Bioelectron.* **2002**, *17*, 53.

[13] a) Y. Hwang, J. Y. Park, O. S. Kwon, S. Joo, C.-S. Lee, J. Bae, *Appl. Surf. Sci.* **2018**, *429*, 258; b) J. S. Lee, S. G. Kim, J. Jun, D. H. Shin, J. Jang, *Adv. Funct. Mater.* **2014**, *24*, 6145; c) W. Zhang, Z. Pan, F. K. Yang, B. Zhao, *Adv. Funct. Mater.* **2015**, *25*, 1588; d) M. A. Darabi, A. Khosrozadeh, R. Mbeleck, Y. Liu, Q. Chang, J. Jiang, J. Cai, Q. Wang, G. Luo, M. Xing, *Adv. Mater.* **2017**, *29*, 1700533; e) B. Weng, A. Morrin, R. Shepherd, K. Crowley, A. J. Killard, P. C. Innis, G. G. Wallace, *J. Mater. Chem. B* **2014**, *2*, 793; f) J. Hur, K. Im, S. W. Kim, J. Kim, D.-Y. Chung, T.-H. Kim, K. H. Jo, J. H. Hahn, Z. Bao, S. Hwang, *ACS Nano* **2014**, *8*, 10066; g) R. Ren, Y. Zhang, B. P. Nadappuram, B. Akpinar, D. Klenerman, A. P. Ivanov, J. B. Edel, Y. Korchev, *Nat. Commun.* **2017**, *8*, 586; h) Q. Li, C. Yu, R. Gao, C. Xia, G. Yuan, Y. Li, Y. Zhao, Q. Chen, J. He, *Biosens. Bioelectron.* **2016**, *80*, 674; i) H. Yoon, S. H. Lee, O. S. Kwon, H. S. Song, E. H. Oh, T. H. Park, J. Jang, *Angew. Chem., Int. Ed.* **2009**, *48*, 2755; j) F. Wei, W. Liao, Z. Xu, Y. Yang, D. T. Wong, C. M. Ho, *Small* **2009**, *5*, 1784; k) J. W. Park, C. Lee, J. Jang, *Sens. Actuators, B* **2015**, *208*, 532; l) R. Ciriello, S. L. Magro, A. Guerrieri, *Analyst* **2018**, *143*, 920; m) J. W. Park, S. J. Park, O. S. Kwon, C. Lee, J. Jang, *Anal. Chem.* **2014**, *86*, 1822; n) A. Shastri, L. M. McGregor, Y. Liu, V. Harris, H. Nan, M. Mujica, Y. Vasquez, A. Bhattacharya, Y. Ma, M. Aizenberg, Y. Ma, M. Aizenberg, O. Kuksenok, A. C. Balazs, J. Aizenberg, X. He, *Nat. Chem.* **2015**, *7*, 447.

[14] L. Pan, H. Qiu, C. Dou, Y. Li, L. Pu, J. Xu, Y. Shi, *Int. J. Mol. Sci.* **2010**, *11*, 2636.

[15] R. Buitrago-Sierra, M. J. García-Fernández, M. M. Pastor-Blas, A. Sepúlveda-Escribano, *Green Chem.* **2013**, *15*, 1981.

[16] a) C.-J. Huang, H.-I. Lin, S.-C. Shiesh, G.-B. Lee, *Biosens. Bioelectron.* **2010**, *25*, 1761; b) A. Bini, S. Centi, S. Tombelli, M. Minunni, M. Mascini, *Anal. Bioanal. Chem.* **2008**, *390*, 1077.

[17] a) Y. Shi, C. Ma, L. Peng, G. Yu, *Adv. Funct. Mater.* **2015**, *25*, 1219; b) W. Bai, N. A. Gariano, D. A. Spivak, *J. Am. Chem. Soc.* **2013**, *135*, 6977.

